# Structural basis for membrane attack complex inhibition by CD59

Emma C. Couves[1], Scott Gardner[1], Tomas B. Voisin[1], Jasmine K. Bickel[1,2], Phillip J. Stansfeld[3], Edward W. Tate[2], Doryen Bubeck[1*]

[1] Department of Life Sciences, Sir Ernst Chain Building, Imperial College London, London SW7 2AZ, United Kingdom

[2] Department of Chemistry, Molecular Sciences Research Hub, Imperial College London, London, W12 0BZ, United Kingdom

[3] School of Life Sciences and Department of Chemistry, Gibbet Hill Campus, The University of Warwick, Coventry, CV4 7AL

*Correspondence to: d.bubeck@imperial.ac.uk

**Supplementary information**

Supplementary Figs. 1-9

Supplementary Table 1

Supplementary Table 2

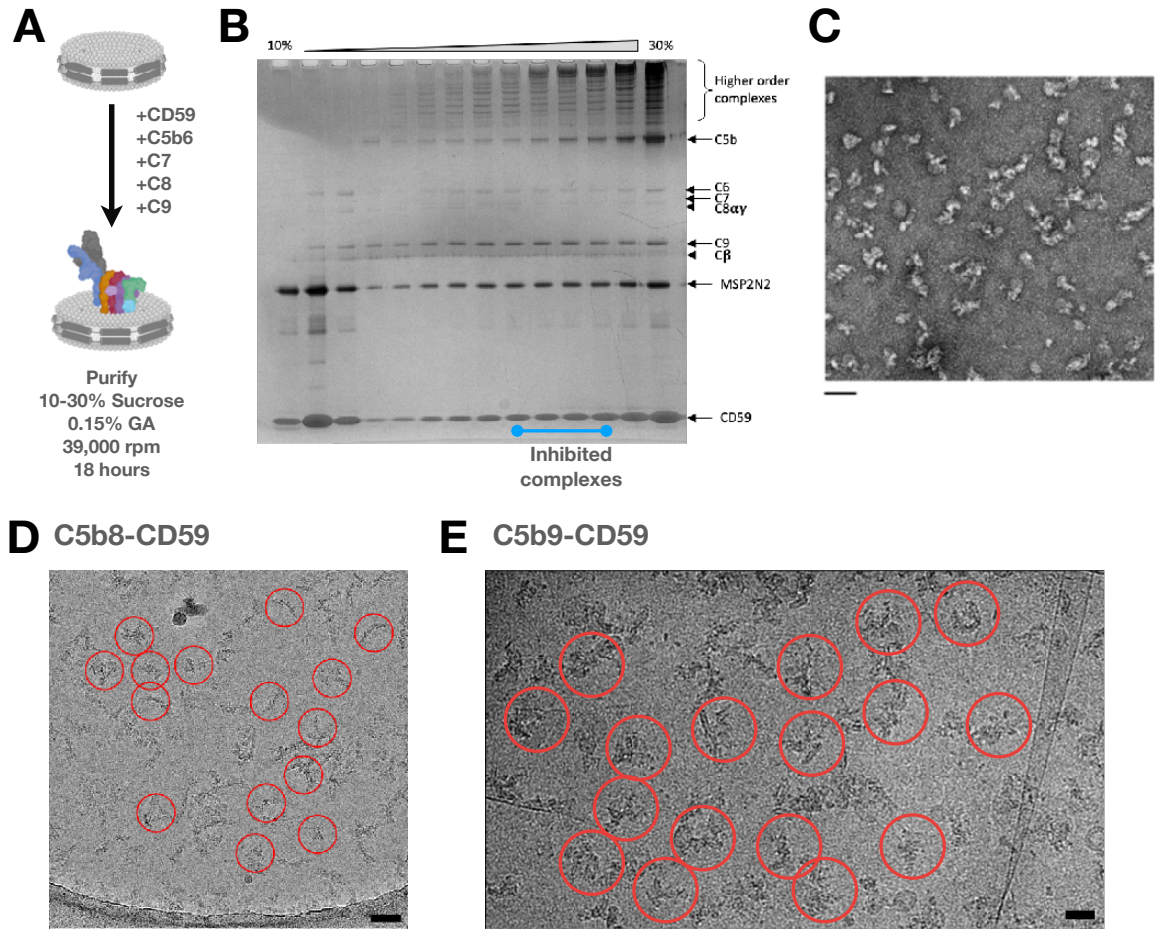


**Supplementary Figure 1**. Supplementary cryoEM data. (**A**) Schematic showing the assembly and purification of CD59-inhibited complement complexes on lipid nanodiscs. Image was created using Biorender (Agreement no: KD24VPIN0O) (**B**) Non-reduced SDS-PAGE gel of fractions along the density centrifugation gradient (10-30% sucrose). Sizes corresponding to individual complement proteins, CD59 and MSP2N2 from the nanodisc are indicated. Fractions pooled for further structural analysis are indicated by a blue line. Gel representative of three independent experiments. Uncropped gel can be found in the Source Data file. (**C**) Negatively stained C5b9-CD59 complexes corresponding to pooled fractions in (B). A representative micrograph from 50 randomly imaged locations is shown. Scale bar, 50 nm. (**D**) Representative cryoEM micrograph of C5b8-CD59 sample (selected randomly from 12,805 micrograph movies), individual complexes circled. Scale bar, 40 nm. (**E**) Representative

cryoEM micrograph of C5b9-CD59 sample (selected randomly from 52,838 micrograph movies), individual complexes circled. Scale bar, 20 nm.

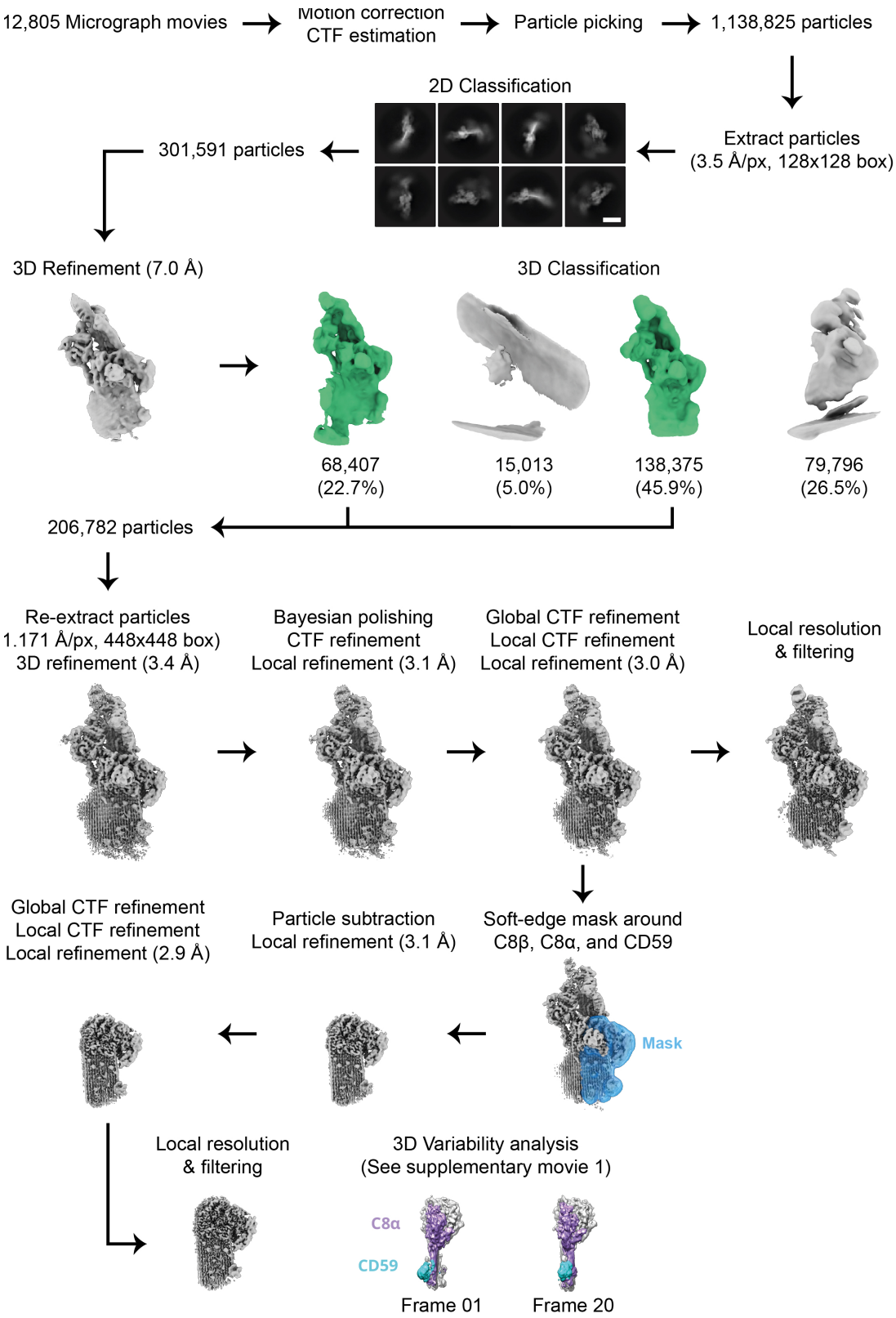

**Supplementary Figure 2**. CryoEM image processing workflow for C5b8-CD59 map. Schematic outlines steps performed to obtain the structure of the C5b8-CD59 complex. Scale bar referring to the 2D class averages is 13 nm. (see Methods for details).

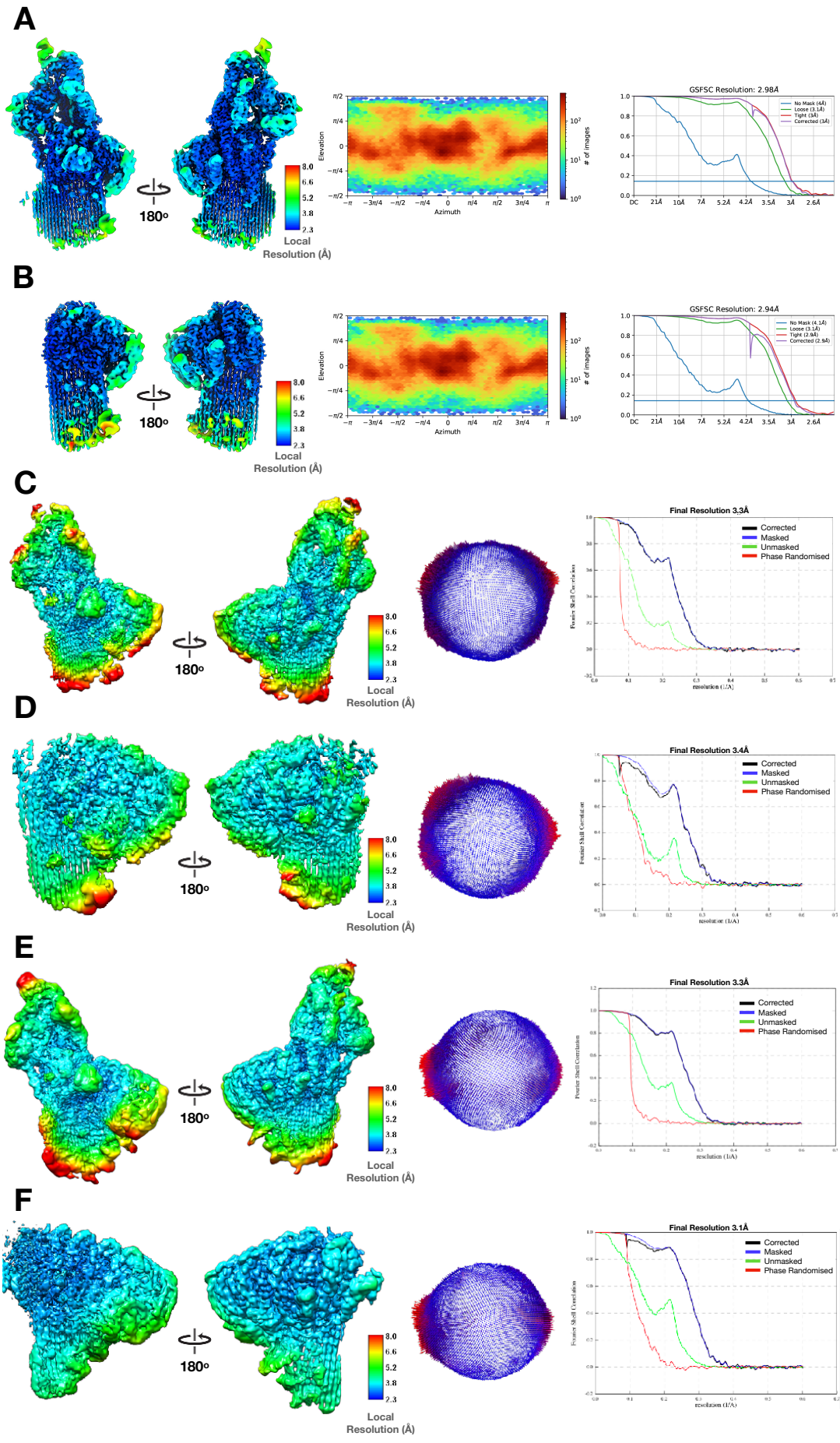
A
180°
8.0
6.6
5.2
3.8
2.3
Local Resolution (Å)
Elevation
Azimuth
# of images
GSFSC Resolution: 2.98Å
No Mask (4Å)
Loose (3.1Å)
Tight (3Å)
Corrected (3Å)
B
180°
Local Resolution (Å)
GSFSC Resolution: 2.94Å
No Mask (4.1Å)
Loose (3.1Å)
Tight (2.9Å)
Corrected (2.9Å)
C
180°
Local Resolution (Å)
Final Resolution 3.3Å
Corrected
Masked
Unmasked
Phase Randomised
D
180°
Local Resolution (Å)
Final Resolution 3.4Å
E
180°
Local Resolution (Å)
Final Resolution 3.3Å
F
180°
Local Resolution (Å)
Final Resolution 3.1Å

**Supplementary Figure 3**. Map validation information for C5b8-CD59 and C5b9-CD59 complexes. Map validations for C5b8-CD59 (**A**), density subtracted focus refined C5b8-CD59 (**B**), C5b9$_2$-CD59 (**C**), density subtracted focus refined C55b9$_2$-CD59 (**D**), C5b9$_3$-CD59 (**E**), density subtracted focus refined C5b9$_3$-CD59 (**F**). Colored local resolution filtered maps for each reconstruction are shown in the left panels. Angular distribution plots for each reconstruction are shown in the middle panels. FSC curves for each reconstruction are shown in the right panels.

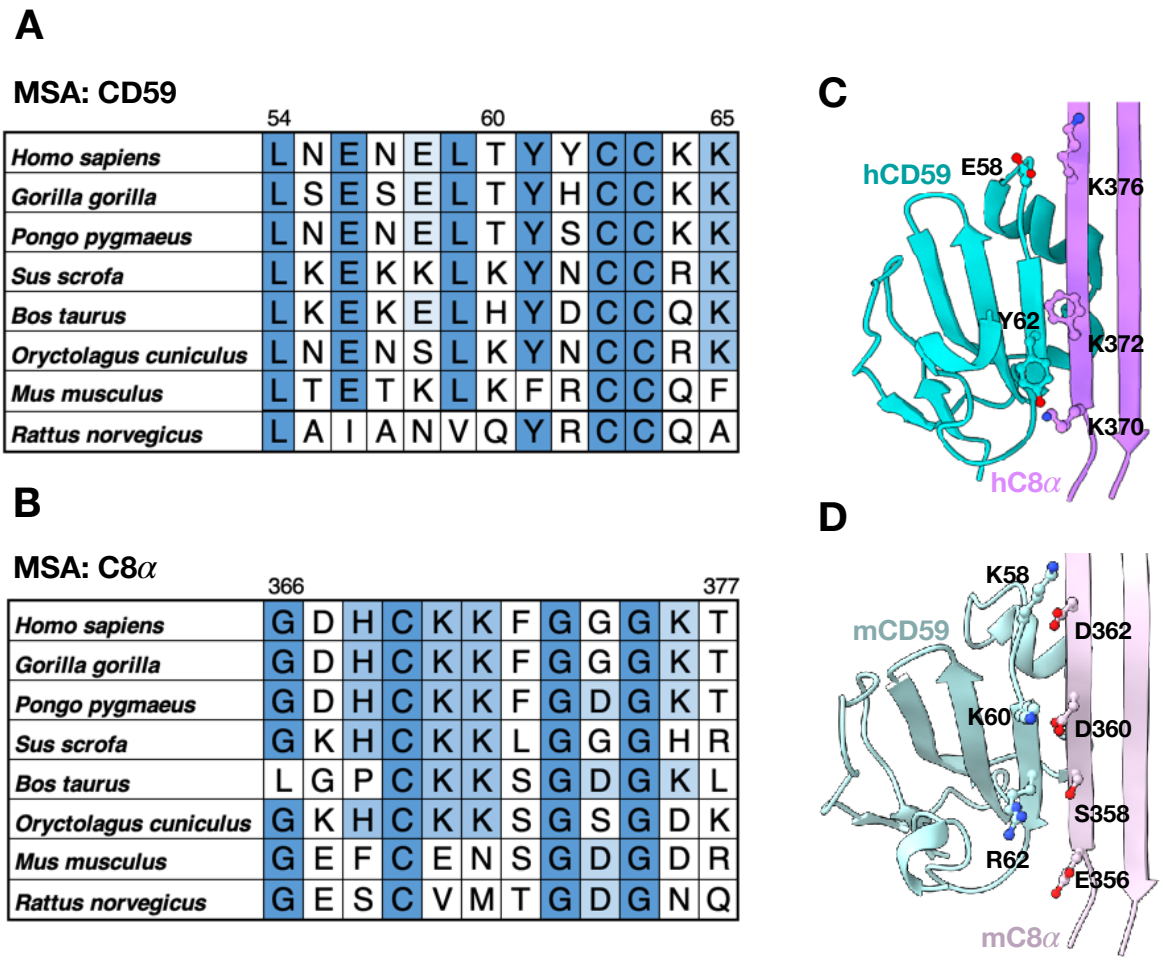


**Supplementary Figure 4**. Co-evolution analysis of the C8α-CD59 interface. Multisequence alignment (MSA) for CD59 (**A**) and C8α residues (**B**) within the binding interface. Numbering corresponds to the human sequence. (**C**) Ribbon diagram of the human C8α-CD59 interface in our structure. (**D**) Murine model of the interface derived from AlphaFold2 prediction of

CD59 (AlphaFold ID: O55186) and template-based model building of C8α. Key residues that mediate the interactions are shown as sticks.

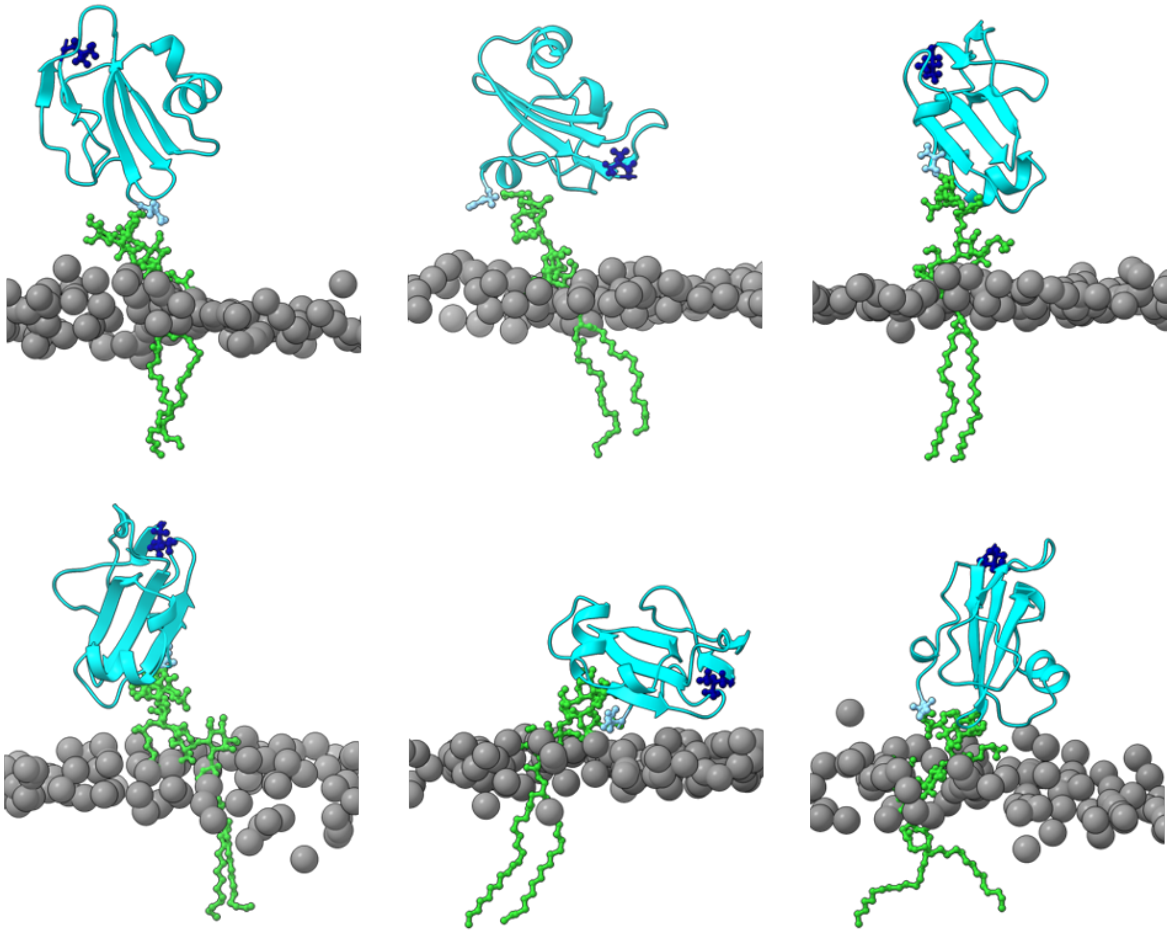

**Supplementary Figure 5**. MD simulations show flexibility of GPI-anchored CD59. Representative frames sampled from the atomistic MD simulations of GPI-anchored CD59 in a DOPC lipid bilayer. CD59 is shown as cyan ribbons with the GPI anchor in green sticks and the N- and C- terminal residues in dark blue and light blue sticks, respectively. Phosphorous atoms from lipid headgroups are grey spheres. Initial and final configurations for the three replicates are supplied as Supplementary Data Files 1-6.

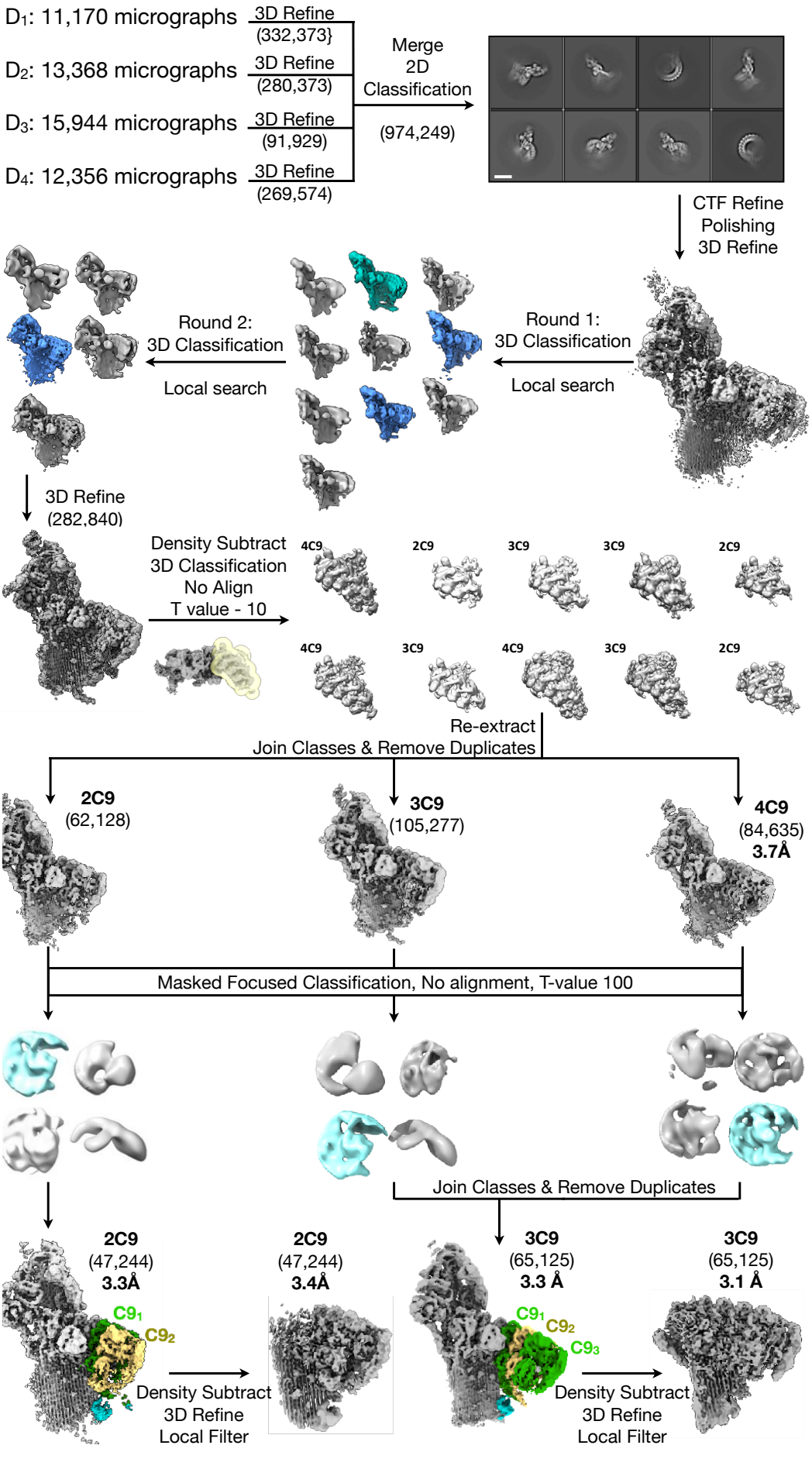
D1: 11,170 micrographs
D2: 13,368 micrographs
D3: 15,944 micrographs
D4: 12,356 micrographs
3D Refine
(332,373}
3D Refine
(280,373)
3D Refine
(91,929)
3D Refine
(269,574)
Merge
2D
Classification
(974,249)
CTF Refine
Polishing
3D Refine
Round 1:
3D Classification
Local search
Round 2:
3D Classification
Local search
3D Refine
(282,840)
Density Subtract
3D Classification
No Align
T value - 10
4C9
2C9
3C9
3C9
2C9
4C9
3C9
4C9
3C9
2C9
Re-extract
Join Classes & Remove Duplicates
2C9
(62,128)
3C9
(105,277)
4C9
(84,635)
3.7Å
Masked Focused Classification, No alignment, T-value 100
Join Classes & Remove Duplicates
2C9
(47,244)
3.3Å
C91
C92
Density Subtract
3D Refine
Local Filter
2C9
(47,244)
3.4Å
3C9
(65,125)
3.3 Å
C91
C92
C93
Density Subtract
3D Refine
Local Filter
3C9
(65,125)
3.1 Å

**Supplementary Figure 6**. CryoEM image processing workflow for C5b9-CD59. Schematic outlines steps performed to obtain the $C5b9_2$-CD59 and $C5b9_3$-CD59 structures. Scale bar referring to the 2D class averages is 20 nm. Particle numbers are in brackets. (see Methods for details).

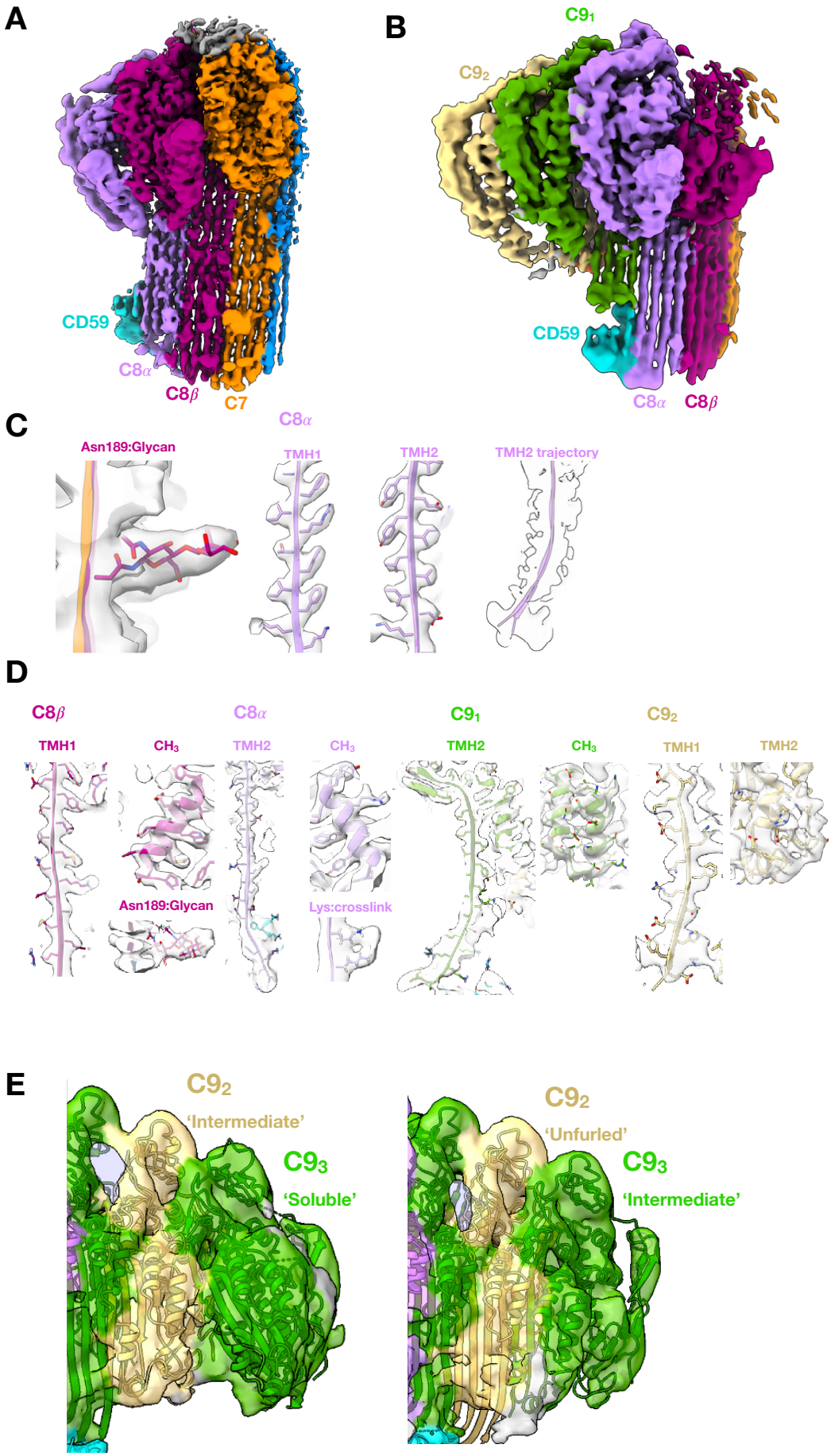
A
CD59
C8α
C8β
C7
B
C9₁
C9₂
CD59
C8α
C8β
C
Asn189:Glycan
C8α
TMH1
TMH2
TMH2 trajectory
D
C8β
TMH1
CH₃
Asn189:Glycan
C8α
TMH2
CH₃
Lys:crosslink
C9₁
TMH2
CH₃
C9₂
TMH1
TMH2
E
C9₂
'Intermediate'
C9₃
'Soluble'
C9₂
'Unfurled'
C9₃
'Intermediate'

**Supplementary Figure 7**. Map quality of the C5b8-CD59 and C5b9-Cd59 structures. (**A-B**) Density subtracted focus refined maps for the C5b8-CD59 (**A**) and $C5b9_2$-CD59 (**B**) complexes. (**C-D**) Fits of the C5b8-CD59 (**C**) and $C5b9_2$-CD59 (**D**) models into their respective density subtracted maps. (**E**) Models for two conformations of the terminal C9 ($C9_3$) derived from the cyroDRGN analysis of the C5b9-CD59 complex.

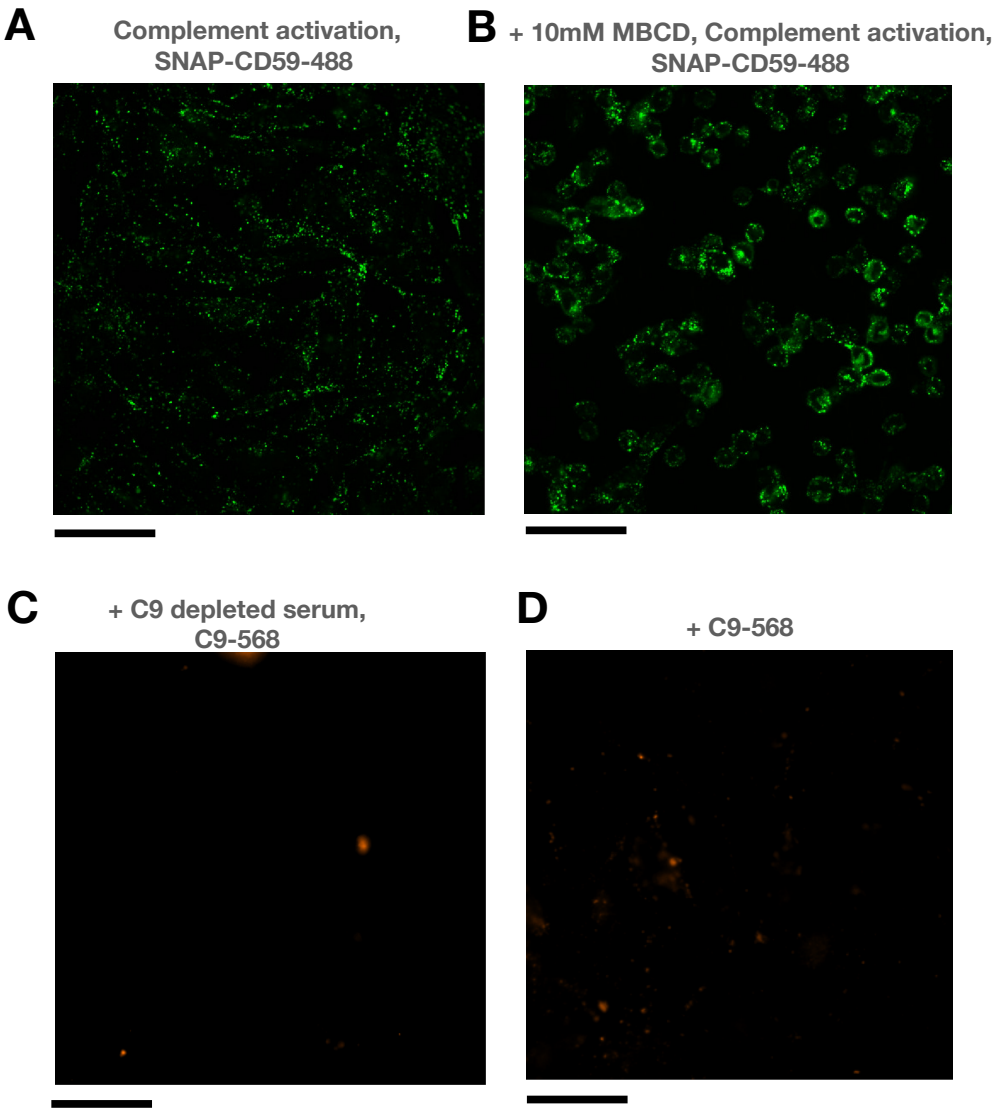
A
Complement activation,
SNAP-CD59-488
B
+ 10mM MBCD, Complement activation,
SNAP-CD59-488
C
+ C9 depleted serum,
C9-568
D
+ C9-568
E
Percentage Cholesterol remaining (%)
120
100
80
60
40
20
0
0
5
10
15
20
25
Concentration of MβCD (mM)

**Supplementary Figure 8**. Supporting cellular assay controls. (**A-B**) CHO cells expressing SNAP-CD59 were treated with a polyclonal anti-CHO IgG antibody to activate complement. Cells were incubated with C9-delpeted human serum supplemented with a chemically-labeled fluorescent C9 (C9-Alexafluor 568) capable of forming MAC. CD59 was visualized with SNAP-Oregon (488 nm) in control cells (**A**) and in cells treated with MβCD to deplete cholesterol (**B**). Wide-field fluorescence microscopy was used to visualize C9 on the cell surface in the absence of complement activator (**C**) and when incubated with C9-Alexafluor 568 alone (**D**). No nonspecific binding is observed. Representative images (out of 10 randomly selected locations) for condition are shown. Scale bars, 50 μm. (**E**) Amplex-Red cholesterol depletion assay detecting the extent of cholesterol present in the cells normalized to untreated cells. Individual measurements are given as points, the average and standard deviation across three technical replicates are shown. Data underlying (**E**) is found in the Source Data File.

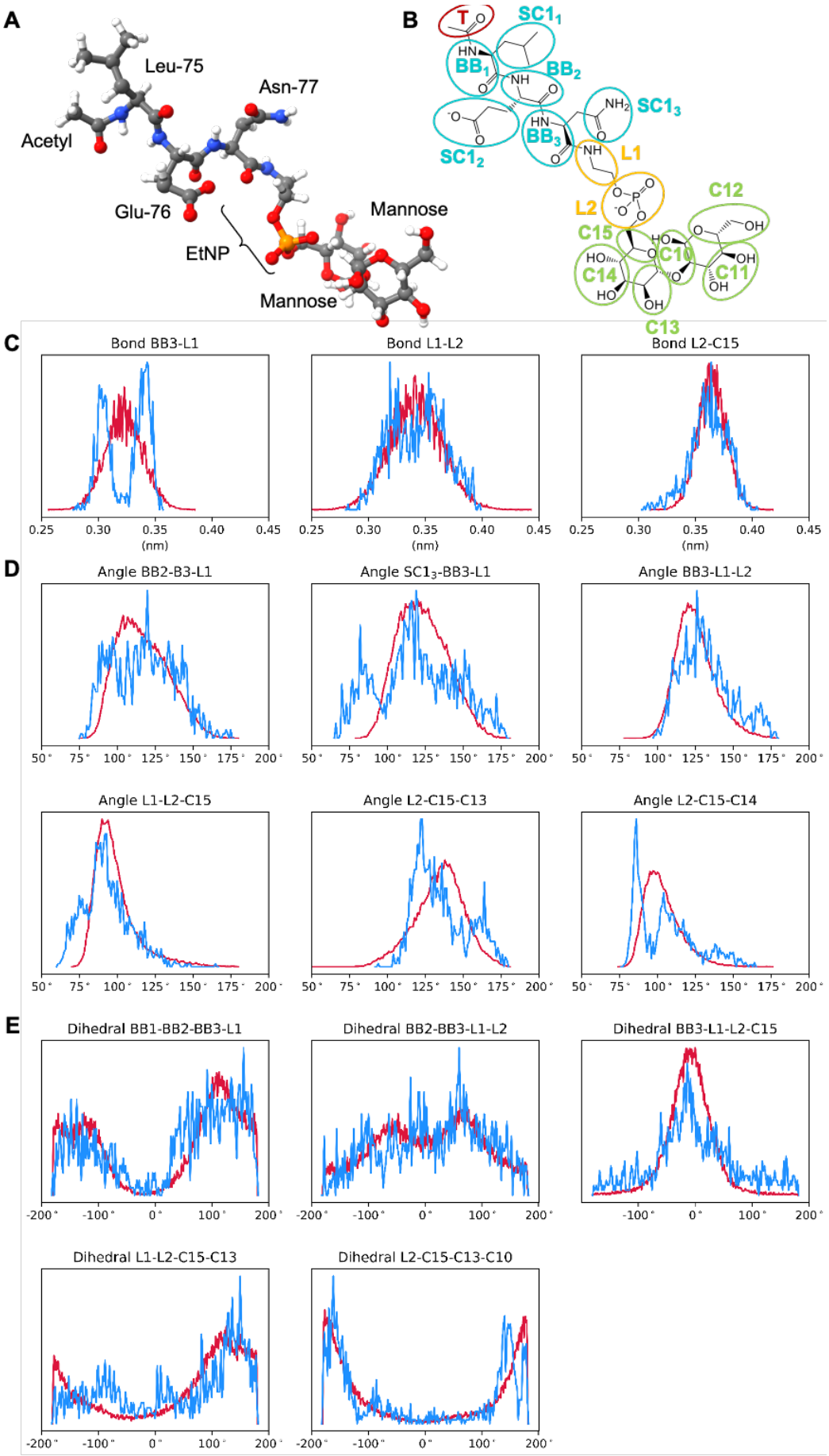
A
Leu-75
Asn-77
Acetyl
Glu-76
Mannose
EtNP
Mannose
B
T
SC1₁
BB₁
BB₂
SC1₃
SC1₂
BB₃
L1
L2
C12
C15
C10
C14
C11
C13
C
Bond BB3-L1
Bond L1-L2
Bond L2-C15
0.25 0.30 0.35 0.40 0.45
(nm)
D
Angle BB2-B3-L1
Angle SC1₃-BB3-L1
Angle BB3-L1-L2
Angle L1-L2-C15
Angle L2-C15-C13
Angle L2-C15-C14
50° 75° 100° 125° 150° 175° 200°
E
Dihedral BB1-BB2-BB3-L1
Dihedral BB2-BB3-L1-L2
Dihedral BB3-L1-L2-C15
Dihedral L1-L2-C15-C13
Dihedral L2-C15-C13-C10
-200° -100° 0° 100° 200°

**Supplementary Figure 9**. Parameterization of the phosphoethanolamine linker (EtNP). (**A**) Stick representation of the molecule used for parameterization. (**B**) Coarse-grained mapping of the molecule in (A). Beads corresponding to the CD59 residues are in cyan, the terminal acetyl cap is red, beads for the EtNP linker (L1 and L2) are in yellow, and beads corresponding to the mannose residues are in green. Comparing bond lengths (**C**) angles (**D**) and dihedral angles (**E**) involving beads L1 and L2 of the EtNP linker between atomistic (blue) and coarse-grained (red) simulations.

**Supplementary Table 1**. Validation statistics for EM maps and models.

| | **#1 C5b8-CD59** EMD: **15779** | **#2 C5b8-CD59$^{arc}$** EMD: **15800** | **#3 C5b9$_2$-CD59** EMD: **15781** | **#4 C5b9$_3$-CD59** EMD: **15780** | **#5 C5b9$_2$-CD59$^{arc}$** EMD: **15782** | **#6 C5b9$_3$-CD59$^{arc}$** EMD: **15783** |
|---|---|---|---|---|---|---|
| **Data collection and processing** | | | | | | |
| **Magnification** | 105k | 105k | 105k | 105k | 105k | 105k |
| **Voltage (kV)** | 300 | 300 | 300 | 300 | 300 | 300 |
| **Electron exposure (e–/Å$^2$)** | 50 | 50 | $D_1$ 43<br>$D_2$ 56<br>$D_3$ 40<br>$D_4$ 50 | $D_1$ 43<br>$D_2$ 56<br>$D_3$ 40<br>$D_4$ 50 | $D_1$ 43<br>$D_2$ 56<br>$D_3$ 40<br>$D_4$ 50 | $D_1$ 43<br>$D_2$ 56<br>$D_3$ 40<br>$D_4$ 50 |
| **Defocus range (μm)** | -1.0 to –2.25 | -1.0 to –2.25 | -1.0 to -2.25 | -1.0 to -2.25 | -1.0 to -2.25 | -1.0 to -2.25 |
| **Detector Type** | Falcon IV | | K3 | K3 | K3 | K3 |
| **Pixel size (Å)** | 1.171 | 1.171 | $D_1$ 0.829<br>$D_2$ 0.831<br>$D_3$ 0.831<br>$D_4$ 0.85 | $D_1$ 0.829<br>$D_2$ 0.831<br>$D_3$ 0.831<br>$D_4$ 0.85 | $D_1$ 0.829<br>$D_2$ 0.831<br>$D_3$ 0.831<br>$D_4$ 0.85 | $D_1$ 0.829<br>$D_2$ 0.831<br>$D_3$ 0.831<br>$D_4$ 0.85 |
| **Symmetry imposed** | C1 | C1 | C1 | C1 | C1 | C1 |
| **Initial particle images (no.)** | 1,138,825 | 1,138,825 | $D_1$ 737,138<br>$D_2$ 1,058,026<br>$D_3$ 1,330,232<br>$D_4$ 722,870 | $D_1$ 737,138<br>$D_2$ 1,058,026<br>$D_3$ 1,330,232<br>$D_4$ 722,870 | $D_1$ 737,138<br>$D_2$ 1,058,026<br>$D_3$ 1,330,232<br>$D_4$ 722,870 | $D_1$ 737,138<br>$D_2$ 1,058,026<br>$D_3$ 1,330,232<br>$D_4$ 722,870 |
| **Particle images before merging (no.)** | N/A | N/A | $D_1$ 332,373<br>$D_2$ 280,769<br>$D_3$ 91,929<br>$D_4$ 269,574 | $D_1$ 332,373<br>$D_2$ 280,769<br>$D_3$ 91,929<br>$D_4$ 269,574 | $D_1$ 332,373<br>$D_2$ 280,769<br>$D_3$ 91,929<br>$D_4$ 269,574 | $D_1$ 332,373<br>$D_2$ 280,769<br>$D_3$ 91,929<br>$D_4$ 269,574 |
| **Final particle images (no.)** | 206,782 | 206,782 | 47,244 | 33,138 | 47,244 | 33,138 |
| **Map resolution (Å)**<br>FSC threshold 0.143 | 3.0 | 2.9 | 3.3 | 3.3 | 3.5 | 3.2 |
| **Map resolution range (Å)** | 2.3-8.0 | 2.3-8.0 | 3.0-12.4 | 3.0-10.2 | 3.1-11.0 | 3.0-8.0 |
| | | | | | | |
| **Refinement** | | | | | | |
| **Initial model used (PDB code)** | 7NYD, 2J8B | 7NYD,2J8B | 7NYD, 2J8B | 7NYD, 2J8B | 7NYD, 2J8B | 7NYD, 2J8B |
| **Model resolution (Å)**<br>FSC threshold 0.5 | 3.0 | | 3.3 | 3.2 | | |
| **Map sharpening** *B* factor (Å$^2$) | -60 | -60 | -50 | -50 | -50 | -50 |
| **Model composition** | | | | | | |
| Non-hydrogen atoms | 30,943 | | 37,288 | 40,505 | | |
| Protein residues | 3910 | | 4704 | 5113 | | |
| Ligands | BMA: 1 | | BMA: 4 | BMA: 0 | | |
| Ions | NAG: 6 | | NAG: 8 | NAG: 10 | | |
| | Ca: 2 | | 0 | 0 | | |
| ***B* factors (Å$^2$)** | | | | | | |
| **Protein** | 86.80 | | 117.93 | 118.03 | | |
| **Ligand** | 136.15 | | 187.03 | 138.05 | | |
| **R.m.s. deviations** | | | | | | |
| Bond lengths (Å) | 0.003 | | 0.001 | 0.009 | | |
| Bond angles (°) | 0.739 | | 0.867 | 0.791 | | |
| **Validation** | | | | | | |
| MolProbity score | 1.81 | | 1.87 | 1.66 | | |
| Clashscore | 4.43 | | 8.53 | 5.49 | | |
| Poor rotamers (%) | 1.4 | | 0.56 | 0.31 | | |
| **Ramachandran plot** | | | | | | |
| Favored (%) | 92.24 | | 95.87 | 94.80 | | |
| Allowed (%) | 7.76 | | 5.13 | 5.20 | | |
| Disallowed (%) | 0.0 | | 0.0 | 0.0 | | |

**Supplementary Table 2**. CG parameters of the molecules used for parametrization of the EtNP linker.

| Bead name | Bead type | Bond | $r_0$ (nm) | $K_b$ (kJ/mol) | Angle | $\theta_0$ (°) | $K_a$ (kJ/mol) |
|---|---|---|---|---|---|---|---|
| T | SN0 | T – $BB_1$ | 0.3 | 20000 | T – $BB_1$ – $BB_2$ | 128 | 20.0 |
| $BB_1$ | P5 | $BB_1$ – $SC1_1$ | 0.33 | 7500 | T – $BB_1$ – $SC1_1$ | 108 | 30.0 |
| $SC1_1$ | C1 | $BB_1$ – $BB_2$ | 0.39 | 20000 | $BB_1$ – $BB_2$ – $BB_3$ | 132 | 30.0 |
| $BB_2$ | P5 | $BB_2$ – $SC1_2$ | 0.4 | 5000 | $SC1_2$ – $BB_2$ – $BB_3$ | 108 | 30.0 |
| $SC1_2$ | Qa | $BB_2$ – $BB_3$ | 0.35 | 20000 | $BB_2$ – $BB_3$ – $SC1_3$ | 96 | 80.0 |
| $BB_3$ | P5 | $BB_3$ – $SC1_3$ | 0.32 | 5000 | $BB_2$ – $BB_3$ – L1 | 105 | 2.5 |
| $SC1_3$ | P5 | $BB_3$ – L1 | 0.33 | 10000 | $SC1_3$ – $BB_3$ – L1 | 90 | 1.0 |
| L1 | GSNda | L1 – L2 | 0.35 | 5000 | $BB_3$ – L1 – L2 | 130 | 60.0 |
| L2 | GQa | L2 – C15 | 0.365 | 18000 | L1 – L2 – C15 | 45 | 5.0 |
| C15 | GNa | C15 – C14 | 0.33 | 20000 | L2 – C15 – C13 | 180 | 15.0 |
| C14 | GP3 | C15 – C13 | 0.35 | 20000 | L2 – C15 – C14 | 70 | 20.0 |
| C13 | GSP1 | C14 – C13 | 0.28 | 40000 | C15 – C13 – C10 | 65 | 45.0 |
| C12 | GP2 | C13 – C10 | 0.36 | 20000 | C14 – C13 – C10 | 95 | 100.0 |
| C11 | GP3 | C12 – C11 | 0.33 | 30000 | | | |
| C10 | GSN0 | C12 – C10 | 0.35 | 30000 | | | |
| | | C11 – C10 | 0.28 | 40000 | | | |

| Dihedral | Type | $\phi_0$ (°) | $K_d$ (kJ/mol) |
|---|---|---|---|
| $BB_2$ – $BB_3$ – L1 – L2 | Proper | 220 | 1.5 |
| $BB_3$ – L1 – L2 – C15 | Proper | –195 | 4.0 |
| L1 – L2 – C15 – C13 | Proper | 320 | 3.5 |
| L2 – C15 – C13 – C10 | Proper | 30 | 3.0 |
| $BB_1$ – $BB_2$ – $BB_3$ – L1 | Improper | –200 | 3.0 |